Nonexponential Unimolecular Decay of Jet-Cooled NO₂: Comparison of Time-Resolved Measurements and Quantum Mechanical Calculations†

Bernd Kirmse and Bernd Abel

Institut für Physikalische Chemie, Universität Göttingen, Tammannstrasse 6, D-37077 Göttingen, Germany

Dirk Schwarzer

Max-Planck-Institut für Biophysikalische Chemie, Am Fassberg 11, D-37077 Göttingen, Germany

Sergy Yu. Grebenshchikov and Reinhard Schinke*

Max-Planck-Institut für Strömungsforschung, Bunsenstrasse 10, D-37073 Göttingen, Germany

We present time-resolved measurements for the dissociative decay of NO₂ in its ground electronic state using pump laser pulses with durations of ca. 650 fs. The temporal evolution of the coherent wave packet is probed by excitation to a Rydberg state and detection of the subsequent fluorescence. The main experimental result is the observation of nonexponential decay, which is most pronounced at very low excess energies close to the dissociation threshold. This is compared with the results of quantum dynamics calculations performed on a recently calculated global potential energy surface. The measured decay curves are satisfactorily reproduced by summation of many exponential decay terms $e^{-k_n t}$, with the state-specific dissociation rates k_n being determined from the widths of resonance poles in the complex energy plane. The key theoretical result is the observation that the calculated rates fluctuate by $1-2$ orders of magnitude. These strong fluctuations are responsible for the distinct nonexponential behavior. The smallest calculated rates just at threshold are of the same order of magnitude, ca. 2×10^{10} s^{-1}, as the experimental rates previously extracted from energy-resolved spectra.

I. Introduction

The microcanonical dissociation rate constant, $k(E)$, is one of the fundamental quantities that characterizes unimolecular decay processes.[1] Because of their (relative) simplicity and their physical insight, statistical approaches for calculating $k(E)$ have received—from the early days of reaction rate theory—considerable attention. The statistical rate is evaluated from the renowned RRKM expression,[2]

$$k_{st}(E) = \frac{W(E)}{h\rho(E)} \tag{1}$$

with $W(E)$ and $\rho(E)$ being the number of open channels and the density of states, respectively, and h is Planck's constant. With the development of computing, classical trajectories have been used to calculate dissociation rates in a more exact fashion.[2,3] The classical dissociation rate, $k_{cl}(E)$, is extracted from the distribution of trajectories that cross the transition state (TS) at a given time. In addition to the statistical and classical methods, numerically exact quantum mechanical calculations of decay rates became feasible in the past decade—at least for small polyatomic molecules (see refs 4 and 5 for recent reviews). In the quantum mechanical approach one calculates scattering-type resonances, i.e., the poles $(E - i\Gamma/2)$ of the **S** matrix in the complex energy plane.[6] The imaginary part, $\Gamma/2$, indicates that these states are metastable and have a finite lifetime τ.

Provided the resonances do not significantly overlap, the quantum mechanical rate constant for a particular resonance state is

$$k_{qm}(E) = \frac{1}{\tau} = \frac{\Gamma}{\hbar} \tag{2}$$

While statistical calculations require knowledge of the potential energy surface (PES) only around the TS region, classical and quantum mechanical studies necessitate a global PES, which covers both the well and the exit channel regions.[7]

Although k_{st}, k_{cl}, and k_{qm}, pertain to the same physical process, their energy dependences can be drastically different. The statistical rate $k_{st}(E)$ is a gradually increasing function of the excess energy E; the higher the energy, the faster the dissociation. The same applies to the classical rate, provided the coupling between the internal degrees of freedom is sufficiently strong. Many experimental examples seem to confirm this general behavior of a gradually increasing rate.[2] However, in quantum mechanics, such an energy dependence can be found only for one-dimensional or spherically symmetric radial problems. If the dissociating molecule has several coupled degrees of freedom, k_{qm} does not depend smoothly on energy, but strongly fluctuates from resonance state to resonance state. The reason is that it is not so much the total energy of the state that determines the rate with which the activated molecule breaks apart but how the energy is distributed among the various degrees of freedom. The average of k_{qm} may rise gradually with E, but the true rates fluctuate around this average.

---

† Part of the special issue "C. Bradley Moore Festschrift".
* Corresponding author. E-mail: rschink@gwdg.de.
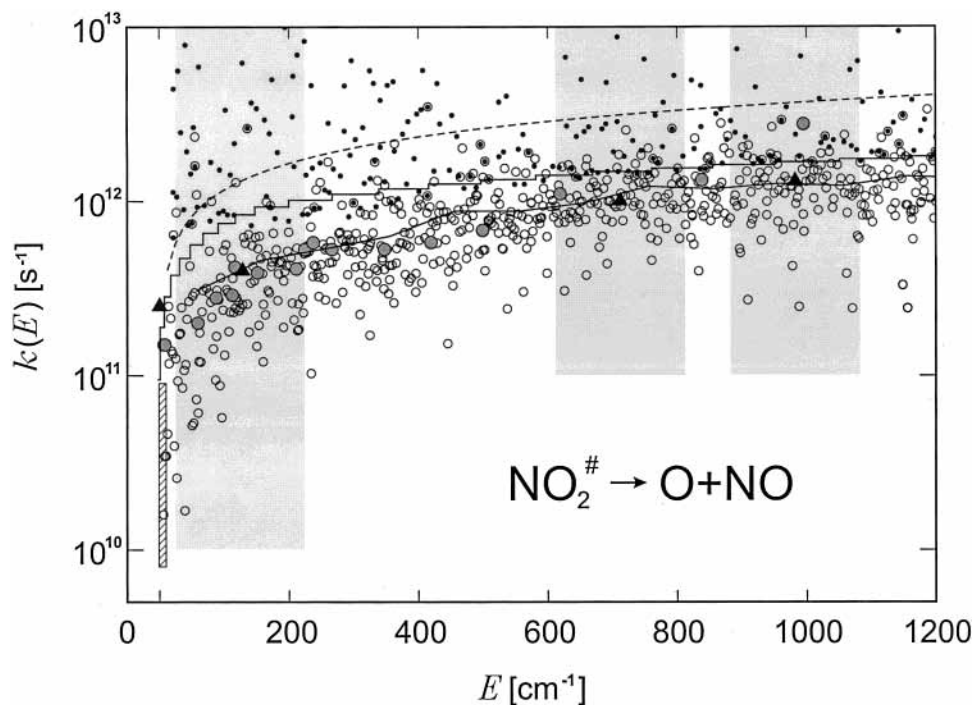
Figure 1. State-resolved calculated dissociation rates as obtained from the resonance poles. Both the well converged (open circles) and the less well converged results (black dots) are shown. The solid line and the broken line indicate the quantum mechanical average ($\Delta E = 200$ cm^{-1}) and the maximum rate obtained from (4), respectively. The solid stepped line is the SACM dissociation rate calculated as described in section III. The triangles represent the experimental average rates obtained in this work and the shaded circles are the rates of Ionov et al.[23] The narrow hatched box at $E = 0$ indicates the range of rates extracted from the energy-resolved spectroscopic experiment by Abel et al.[20] The shaded boxes ($\Delta E = 200$ cm^{-1}) indicate the ranges of resonance states excited by the pump pulses with λ_{pu}, 387 and 383 nm, respectively.

Figure 1 provides an example of such behavior, the state-specific quantum mechanical rate constants for the dissociation of NO₂ in its ground electronic state. States, which are almost degenerate, may have rates differing by orders of magnitude. This is a direct result of the multidimensionality of the underlying molecular dynamics.[8] The fluctuations are especially pronounced near the threshold, $E \approx 0$, where they exceed 2 orders of magnitude. Figure 1 is the main result reported in the theoretical part of this paper. The key experimental result is that these fluctuations are sufficiently large for being experimentally discernible: For excess energies up to 1000 cm^{-1} above threshold, the time-resolved decay of vibrationally excited NO₂ is distinctly nonexponential. The deviations from single-exponential decay are too strong to be explained by the smooth energy dependence of $k_{st}(E)$ across the energy windows probed by the laser pulse. They are the *direct* consequence of the wide variation of dissociation rates of resonance states simultaneously excited by the laser.

Fluctuations of dissociation rates have been previously investigated for other triatomic molecules.[4] The range of the fluctuations depends markedly on the coupling between the intramolecular modes. It is large (4−7 orders of magnitude) if the coupling is weak like for HCO[9,10] and HOCl,[11,12] and it reduces to 1−2 orders of magnitude, if the dynamics is irregular as for HNO[4] and NO₂ (Figure 1).

Adequate experimental tools for studying the decay dynamics depend on the density of states and the average resonance width. If the resonances are well separated, frequency-domain spectroscopy is the method of choice for determining the resonance widths, Γ, and the associated state-specific rates. Experimental results have been reported for D₂CO,[13] HCO,[9] DCO,[14] CH₃O,[15] HOCl,[16,17] and HONO.[18] In all these examples, the rates are found to strongly fluctuate from one vibrational−rotational state to another. If the average resonance width exceeds the mean

spacing between neighboring resonances, extracting rates from a spectrum is unreliable or not possible at all. For NO₂ with $\Delta E = \rho^{-1} \sim 1.5$ cm^{-1} at threshold, line widths could be resolved only in a tiny interval of approximately 10 cm^{-1} above threshold;[19,20] at higher energies the absorption lines broaden and overlap and can no longer be analyzed.

If individual resonances cannot be resolved spectroscopically, the experimental information about dissociation rates can be inferred from a time-resolved measurement.[21] In a pump−probe experiment[22] a first laser pulse with wavelength λ_{pu} prepares a coherent wave packet with a mean energy, which is larger than the dissociation threshold. After a certain time delay, Δt, either the disappearance of the excited parent molecule or the appearance of the products is probed with a second laser with wavelength λ_{pr}. For NO₂, the latter scheme has been previously adapted by Ionov et al.[23] and the dissociation rate has been measured up to an excess energy of about $E = 1000$ cm^{-1}. A single-exponential ansatz was found to be sufficient to model the measured buildup curves and to extract rates.

In the present article we report new time-resolved measurements. The studied range of excess energies is roughly the same as in ref 23; however, instead of monitoring the buildup of the NO fragment, the disappearance of the parent molecules is *directly* monitored. In contrast to the results of Ionov et al.[23] we find distinct nonexponential decay, with the deviation from single-exponential behavior being most pronounced at small excess energies. The accompanying quantum mechanical calculations, employing a global potential energy surface for the ground electronic state,[24] undoubtfully support this observation and are in good overall agreement with the experimental decay curves.

NO₂ is a benchmark system for experimental as well as theoretical investigations of unimolecular dissociation.[2] The spectroscopy, photodissociation, and kinetics have been studied

in great detail by many research groups (see ref 25 for a recent review). The electronic spectroscopy has been unraveled by Smalley et al.[26] Single-photon excitation, promoting NO_2 above the first dissociation threshold, produces $NO(^2\Pi_\Omega)$ and $O(^3P_J)$ with $\Omega = 0.5$ and 1.5 and $J = 0-2$. A number of groups have examined the UV photodissociation, reporting kinetic energy and angular distributions,[27] state-resolved product distributions,[25,28−30] photofragment excitation spectra,[19] zero-kinetic energy photofragment spectra,[31] and double resonance spectra of highly excited NO_2 close to threshold.[20] Some time ago, Gaedtke et al.[32] measured photodissociation quantum yields and reported reaction rates using collisions as an internal clock. At high excess energies the lifetime of NO_2 has been determined from measurements of the product angular distribution and the alignment of the rotational angular momentum with respect to the fragment recoil velocity.[33] Very recently, anisotropy parameters have been determined also at energies near threshold by Monti et al.[34]

It is worth mentioning that fluctuations in various observables, especially in the product state distributions and anisotropy parameters, are common to several of the experiments, particularly the more recent ones. This aspect has been extensively discussed, for example, by Reisler and co-workers.[25] The present work extends this observation into the domain of state-specific reaction rates.

NO_2 is small enough to permit detailed calculations and there are many theoretical studies of the electronic excitation,[35] the bound states,[36−39] the vibrational wave packet dynamics,[40] and the unimolecular dissociation.[24,41,42] However, fully quantum mechanical calculations of the dissociation rates, necessary for comparison with the time-resolved fragmentation measurements, have not been presented yet.

The paper is organized in the following way: The experimental approach is described in section II, and the calculations are briefly outlined in section III. The multiexponential decay, the large fluctuations of the calculated widths, and the comparison between theory and experiment are discussed in section IV. Finally, the main conclusions are summarized in section V. The details of the theoretical model are subject of an accompanying paper,[43] which hereafter we will refer to as paper II.

II. Experimental Approach

A. Pump/Probe Scheme. The experiments are performed in a molecular beam. The rotational temperature is ca. 3−5 K. The initial vibrational excitation is negligible; even at room temperature the excitation of the first excited vibrational level is less than 2%.

The pump/probe scheme used in the experiment is schematically depicted in Figure 2 together with the relevant electronic states of NO_2. Two lasers with wavelengths λ_{pu} and λ_{pr} and pulse durations shorter than 1 ps are employed. The first laser is used to excite NO_2 to states slightly below, above, or far above the first dissociation threshold. With one-photon optical pumping, states which are mixtures of the $^2A_1$ and $^2B_2$ zeroth-order doublet electronic states are populated. For spectroscopic details in this wavelength region we refer to ref 20. The time dependence of the decay, i.e., the depletion of the population of the parent molecule, is directly probed with λ_{pr}. The highly vibrationally excited NO_2 molecules are, after a time delay Δt, further excited by the second laser with a wavelength close to 310 nm to the Rydberg states $^2\Pi_g^+$ and $^2\Sigma_u^+$. The existence of these states, which lie in the energy range 54 000−56 000 cm^{-1}, is of extreme importance for the proposed experimental scheme.
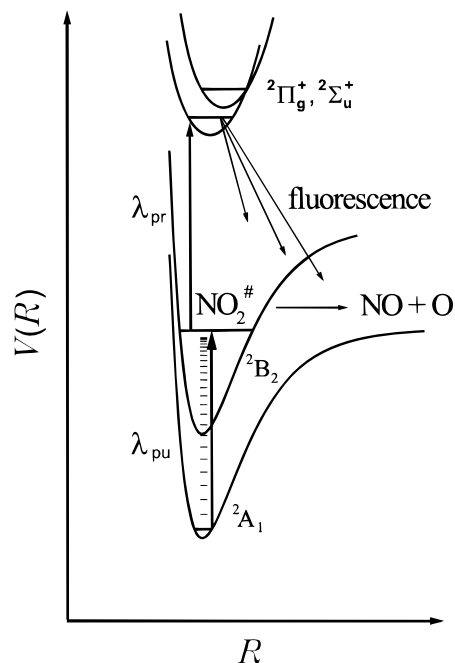
Figure 2. Scheme of the pump−probe experiment.

Their spectroscopy has previously been investigated by Bigio and Grant by means of ionization.[44] We have recently discovered that these states fluoresce in the UV spectral range and the observed fluorescence below 320 nm (UG11 filter) is used as a measure of the population of the highly excited states at time Δt.

Molecules which do not dissociate, because their internal energy is below D_0, are also detected, and therefore the LIF signal does not necessarily decay to zero with increasing Δt. If λ_{pr} is chosen so that only bound states are excited, a signal, which does not decay at all, is observed. In this case the rise time of the signal represents the cross correlation of the two laser pulses. The width of the cross correlation function is about 650 fs in our experiments. The Franck−Condon factors for the states that are pumped and for the states that are probed have been found to be very similar over a range of pump and probe wavelengths. We have checked this in a series of measurements in which λ_{pu} and λ_{pr} have been varied: no significant changes in the intensities of transitions have been observed. Considering that relatively short laser pulses are used, one might worry whether the same states are pumped and at a later time probed. Because the mixing time between the two electronic states and the internal vibrational energy redistribution (IVR) time are both considerably shorter than the laser pulse durations, we are quite confident that the wave packet, that is created after the pump pulse is switched off, is a random superposition of all resonance states in the relevant energy window. In coordinate space, it spreads with a random-like nodal structure over the entire coordinate space accessible. Although the wave packet will change its shape during the time delay Δt, the general form will remain the same.

It has been checked that the intensities of the fluorescence signals depend linearly on the energies of the pump and the probe pulses, such that two-photon excitation or a multiphoton probe are avoided. The time resolution of the laser system has been found to depend strongly on the excitation wavelength selected from the continuum, which was generated from 620 nm of the CPM oscillator (see below). It ranges from 180 to 650 fs (cross correlation). Most of the measurements discussed in this paper have been performed with a time resolution (not

optimized) of about 650 fs. This time resolution has been found to be sufficient, because at excess energies between 0 and 1000 cm^{-1} the average dissociation rate is much slower than $1 \ ps^{-1}$. During the experiment the cross correlation and the time of zero delay have been determined via difference-frequency generation in a thin BBO crystal and the spectra of the pump and probe pulses have been routinely recorded with a spectrograph equipped with a CCD array detector. A typical spectral width for the 650 fs pulses is $200 \ cm^{-1}$ (fwhm), which is larger than the Fourier limit for them. A single experiment has been performed with $\lambda_{pu} = 310$ nm and $\lambda_{pr} = 620$ nm with a time resolution of 180 fs. For this wavelength the average dissociation rate is faster than $1 \ ps^{-1}$, and therefore a much shorter pulse is essential.

B. Experimental Setup. The home-built laser system is based on a colliding-pulse mode-locked ring dye laser (CPM) pumped by an argon ion laser. It generates $70-130$ fs pulses at 620 nm with a spectral bandwidth of about 10 nm. The standard configuration of the oscillator consists of an absorber (DODCI) and a gain jet (Rhodamine 6G), four folding mirrors, two reflecting dichroic mirrors (0°, 620 nm), as well as a sequence of four prisms in a Brewster-angle configuration for the compensation of the group velocity dispersion. The cavity length of the ring laser is set to obtain a repetition rate of 76 MHz. The CPM laser oscillator is synchronized with an injection seeded 20 Hz Nd:YAG laser (Continuum, NY81-20) so that pulses from the CPM-laser can be amplified at a repetition rate of 20 Hz. The pulses from the oscillator are amplified by a standard three stage system (two transversely excited cells and a Bethune-cell with Rhodamine 101 and Sulforhodamine in methanol), which is pumped by 60 mJ (5%, 15%, and 80% for the different stages) of the second harmonic of the Nd:YAG laser. To minimize amplified spontaneous emission (ASE), we employ a thin flow cell with Malachit Green solved in methanol as a saturable absorber and 200 μm pinholes in order to spatially filter the laser pulse profile. After the three-state amplification of the 616 nm fundamental of the CPM laser a standard pulse energy of $100-200 \ \mu$J is obtained. Subsequently, the pulse has to be recompressed; i.e., the positive group velocity dispersion (GVD) has to be compensated. This is achieved with a standard four prism arrangement (SF10) or two prisms, where each prism is passed twice. The recompressed fundamental of the CPM (100 fs, 100 μJ at 616 nm) is split into two parts with a 50% beam splitter and both pulses are focused ($f = 200$ mm) into two different thin water cells in order to generate a white light supercontinuum. The desired wavelengths are selected with two interference filters (5 or 10 nm, fwhm). The two pulses are then amplified in two independent three-stage amplification chains, which are pumped by the second and third harmonics of the seeded Nd:YAG laser and recompressed in a four-prism arrangement. Typically $50-100 \ \mu$J can be generated in the wavelength range between 800 and 380 nm. Light in the UV spectral range down to 220 nm is obtained by doubling the amplified laser pulses selected from the continuum. For the doubling we use 200 μm KDP and a BBO crystal from Gsänger Optics.

After passing a delay stage the probe pulse is combined and overlapped with the pump laser pulse using dichroic mirrors. Both slightly focused laser beams pass collinearly the vacuum recipient containing the free jet or a thermal sample of NO₂ seeded in Ar ($1-5\%$).

Finally, the laser-induced fluorescence in the UV spectral range is collected with $f/1.2$ optics and detected with a solar-blind photomultiplier (Hamamatsu R166). Scattered light is suppressed by using a UG11 filter and a slit (for spatial filtering of the LIF) in front of the multiplier. For the jet experiments the vacuum chamber is equipped with a pulsed nozzle (General Valve IOTA 1, 200 μm orifice) and a quadrupole mass spectrometer to monitor the jet. For data acquisition we use a personal computer, which collects the data and all laser pulse energies and controls the delay stage.

III. Theoretical Approach

The dissociation dynamics is studied using the lowest *adiabatic* PES of NO₂, which has been discussed in detail in ref 24. The PES has mainly the character of the ground electronic state. It has been calculated by ab initio methods at the CASPT2 level.[24] It is a global potential; i.e., the ab initio points cover both the inner and the asymptotic regions over a wide range of ONO bending angles. The calculated fundamental frequencies, the dissociation energy, and the density of bound states are in reasonable agreement with known experimental data. Moreover, dissociation rates extracted from classical trajectory calculations are in good accord with the experimental results of Ionov et al.[23]

Rigorously speaking, a complete description of the unimolecular dissociation of NO₂ would involve global potential energy surfaces for at least the ground, $\tilde{X}^2A_1$, and the first excited electronic state, $\tilde{X}^2B_2$, and the corresponding matrix elements of the nuclear kinetic energy operators, which couple them.[35] The main role of the vibronic coupling is to mix the initially excited vibrational levels on the $\tilde{X}^2B_2$ state PES with the highly vibrationally excited irregular states of the $\tilde{X}^2A_1$ manifold.[45,46] The time of mixing, τ_{mix}, is less than 100 fs for excitation near the maximum of the absorption spectrum,[45] which is considerably shorter than the average dissociation time at small excess energies. Therefore, we believe that following the evolution of the system on the ground-state PES alone provides a realistic description of the unimolecular dissociation process. The vibrational dynamics at energies near the threshold is chaotic irrespective of whether the excited electronic state is taken into account.[24] In view of the restriction to the ground state, times shorter than τ_{mix} cannot be considered within our model and calculated dissociation rates larger than τ_{mix}^{-1} are not meaningful. As we shall see in the next section, this is a rather mild limitation that does not influence the comparison with experimental decay curves.

The dissociation dynamics for total angular momentum $J = 0$ is studied by calculating the time evolution of a wave packet $\Phi(t)$ (see, for example, ref 7). The time evolution operator is expanded in terms of Chebyshev polynomials $\hat{Q}_n$ modified as suggested by Mandelshtam and Taylor.[47] The modified $\hat{Q}_n$'s contain a real coordinate-dependent damping factor, which makes the (expanded) evolution operator equivalent to the evolution operator of an optical model. Namely, the dynamics of the wave packet is governed by an effective Hamiltonian of the form

$$\hat{H}_{opt}(E) = \hat{H} - i V_{opt}(E) \qquad (3)$$

where $\hat{H}$ is the Hamiltonian of a triatomic molecule, and $iV_{opt}(E)$ is the positive-definite imaginary (optical) potential, which absorbs those parts of the wave packet that approach the edge of the three-dimensional grid used to represent $\Phi(t)$, and thereby prevents spurious reflections. In addition to the dependence on the internal coordinates, the optical potential depends explicitly on the energy E. The advantage of the modified Chebyshev polynomials over conventional methods[7] is that

extremely long time steps can be applied. The overlap integrals c_n of the initial wave packet $\Phi(0)$ with the Chebyshev vectors $\hat{Q}_n\Phi(0)$ are stored during the calculation. The sequence $\{c_n\}$ is subsequently analyzed by means of the harmonic inversion method[48,49] to yield a set of complex eigenvalues $(E_n^0 - i\Gamma_n/2)$ of the Hamiltonian $\hat{H}_{opt}$. The autocorrelation function $S(t) = \langle\Phi(0)|\Phi(t)\rangle$, required in the standard approach for calculating a spectrum,[7] can easily be reconstructed from the set $\{c_n\}$. However, in the present case it has no direct physical meaning, because the wave packet at $t = 0$ is defined as a random distribution on the three-dimensional spatial grid. We use a randomly defined $\Phi(0)$ (and not a localized Gaussian-type wave function as commonly employed in photodissociation studies) in order to guarantee that as many resonance states as possible are contained in this initial wave packet. The construction of theoretical decay curves, which can be compared with the measurements, is described in the next section.

The wave packet is represented in the Jacobi coordinates R, the distance between the O atom and the center-of-mass of the NO diatom, r, the NO separation, and γ, the angle between $\vec{R}$ and $\vec{r}$ with $\gamma = 180°$ corresponding to linear ONO. The Hamiltonian, including the absorbing potential, is defined in a discrete-variable-representation (DVR) basis.[50] Several calculations have been performed in order to optimize the grid size and the strength of the absorbing potential in R and r. In the largest calculation we use 200 sinc-DVR points in the interval $2\ a_0 \leq R \leq 15.5\ a_0$. For the r coordinate, 200 sinc-DVR points in the interval $1a_0 \leq r \leq 13.5\ a_0$ are initially set and subsequently contracted to 100 points by use of the HEG method;[51] for the angular coordinate we use 100 Gauss–Legendre DVR points. The number of Chebychev iterations is 400 000. The average energy of the random wave packets used in the propagation is about 3.0 eV, while their energetic width is of the order of 4 eV. Consequently, one can extract *all* resonance energies in the energy range of interest ($E \leq 2000$ cm^{-1}) from a *single* quantum propagation. More details about the calculations will be given in a separate article.[52]

Extraction of the resonance data from the signal $\{c_n\}$ by means of the harmonic inversion method is not error free. The resulting resonance energies and widths are subject to some uncertainty. In our calculations, the uncertainties are insignificant for the narrow resonances and largest for the widths of the broad resonances. To assess the influence of the broader resonances on the decay curves, we produced two sets of resonances by applying two different convergence criteria for the widths. The main set contains only those resonance poles whose real and imaginary parts have uncertainties of less than 5% and 20%, respectively (open circles in Figure 1). Resonances with widths $\Gamma \geq 10$ cm^{-1} or so (corresponding to rates larger than about 2×10^{12} s^{-1} or lifetimes shorter than about 0.5 ps) are underrepresented in this spectrum. Therefore, this first list is augmented by also taking into account resonances for which the convergence criterion is relaxed from 20% to 50% for the widths. They are shown in Figure 1 with black dots. If the distance between two states in the complex plane happens to be smaller than the uncertainty in their positions, both are assumed to represent a single resonance. Although this second set is of lower numerical quality, it helps us to illustrate the breadth of the resonance distribution in NO$_2$: broad resonances coexist with narrow ones in virtually any energy region.

The convergence criterion with respect to the harmonic inversion method is not fully sufficient for deciding which poles of the Green operator should be taken into account or neglected. Poles, which are too broad, have wave functions extending all

the way to the end of the grid in R. These resonances are impossible to converge, with respect to R_{max} and the onset of the absorbing potential, and they correspond to direct scattering states rather than quasi-bound states localized in the potential well. In principle, each resonance wave function should be checked in order to select the true resonance states. However, because the energies are not obtained by diagonalization of a matrix, the calculation of many wave functions is cumbersome and prohibitively time-consuming. A careful analysis of HOCl dissociation—this molecule is similar to NO$_2$ in that a heavy atom is split off and that the PES has no barrier—has revealed that only resonances with widths below a certain upper limit,

$$\Gamma_{max} = \frac{2\hbar\sqrt{2E/\mu_R}}{R_{max}} \qquad (4)$$

can be converged with respect to the end of the grid, R_{max}, and therefore should be further considered. The square root in this equation is the velocity v_R of a free particle with mass μ_R and energy E, and thus the maximum width corresponds to the time it takes a ballistic particle to fly across the grid. Only poles with $\Gamma < \Gamma_{max}$ are included in the subsequent calculation of decay curves.

To estimate the applicability of statistical theories, we will compare the experimental and the quantum mechanical decay curves with the predictions of the statistical adiabatic channel model (SACM).[53] In the SACM approach adiabatic potential curves $\epsilon_{n,j}(R)$ are required, where n and j are the vibrational and rotational quantum numbers of the NO fragment, respectively. For NO$_2$, they have been determined using the same PES as employed in the quantum mechanical calculations.[24] The number of open fragment channels, $W(E)$, for an excess energy E is defined as the total number of adiabatic states, which are below E all the way from the inner to the asymptotic region of the potential. The energy dependent rate constant is given by eq 1. While the number of open channels is well-defined for a given PES, the density of states, $\rho(E)$, in the continuum is not unique. As in the classical study,[24] $\rho(E)$ is estimated by extrapolation from the bound part of the spectrum into the continuum.[54]

IV. Results

A. Time-Resolved Dissociative Decay of Jet-Cooled NO$_2$. The experimental decay curves are displayed in Figure 3 for four mean excess energies $\bar{E} = \hbar\omega - D_0$. The amplitude of the signal at $t = 0$ is a measure of the total number of the excited molecules. The experimental data in Figure 3 are processed in three steps. First, a small background resulting from NO fluorescence from the 310 nm probe pulse is subtracted. Second, only those data points are accepted, for which the pump and probe laser energies are nearly constant and vary only within narrow energy windows. Finally, each trace is normalized so that its maximum equals to 1.

The pump pulse with the longest wavelength, $\lambda_{pu} = 398$ nm, excites states in an energy window centered around the dissociation energy; i.e., the average excess energy is approximately zero. NO$_2$ is promoted to states both below and above the dissociation threshold. As a result, the signal does not vanish at large times but levels off at roughly 30% of the original intensity at $t = 0$. For the next higher excess energy, $\bar{E} \sim 124$ cm^{-1}, the laser pulse excites substantially more continuum states than bound states with the consequence that the decay curve approaches a smaller asymptotic value. For the two highest excess energies only resonances above the dissociation
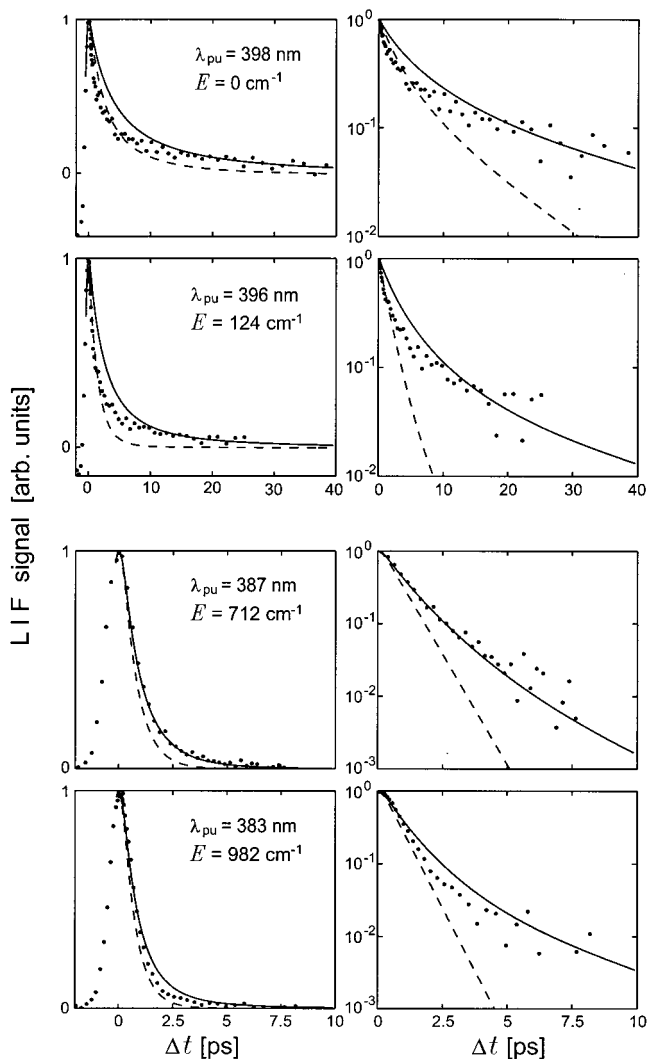
Figure 3. Time dependent decay curves depicted on linear (left-hand panels) and on logarithmic (right-hand panels) scales: dots, experimental results; solid lines, quantum mechanical decay curves obtained from the resonance poles; dashes, statistical decay curves obtained from the SACM rates. Note the different time scales. See the text for further details.

threshold and no bound states are excited such that all excited molecules dissociate. The decay is significantly faster than for the two lower excess energies (note the different time scales). Although the decay curves rapidly fall off to zero, the time resolution is still sufficient to discern the delay due to molecules with lifetimes larger than the pulse length; both signals are clearly asymmetric with respect to $t = 0$.

The logarithmic representations depicted in the right-hand panels of Figure 3 clearly show that the decay curves are *nonexponential*.[55] This is most pronounced for the lowest two energies. At the two higher excess energies, the short-time portions of the decay traces ($t \leq 2$ ps) can be fitted with a single exponential. However, when the population drops below 10% of the initial value, a multiexponential fit becomes necessary. The nonexponential decay is an important finding in the present experiments. It is the straightforward and obvious consequence of the pronounced state specificity of the dissociation dynamics[4] and the resulting strong fluctuations of the state-resolved dissociation rates. The decay curves, therefore, are much more informative than a single average decay constant.

B. State-Specific Quantum Mechanical Decay Rates. The imaginary parts, $\Gamma_n/2$, of the calculated resonance energies are

converted into state-specific dissociation rates k_n according to eq 2 and plotted against the excess energy in Figure 1 (see also Supporting Information). The two sets of rates corresponding to the two sets of calculated resonances with different convergence criteria are distinguished by different symbols. Most rates belonging to the better converged set of resonances correspond to lifetimes longer than 1 ps.

The calculated rates fluctuate strongly around an average value. Close to the threshold, k_n spans more than 2 orders of magnitude, even if we take into consideration only those poles determined with the more severe convergence criterion. With increasing excess energy the variations of k_n in a given energy window shrink to about 1 order of magnitude. The importance of these large-scale fluctuations for the molecular dynamics can be perceived from the fact that the difference in the decay rates of two successive states may well exceed the overall growth of the average rate in the whole energy interval studied.

Fluctuating dissociation rates have been observed in recent years for several small molecules and have been found in several quantum mechanical studies (see ref 4 for references); i.e., their existence is well established. Nevertheless, in view of the relatively large density of states ($\rho \approx 0.6/\text{cm}^{-1}$ at threshold) and the chaotic classical dynamics already far below the fragmentation limit, the large degree of fluctuations for NO$_2$ comes as a surprise. It should be noted that the resonance states cannot be assigned in terms of vibrational quantum numbers; the corresponding resonance wave functions, some of which have been calculated, are spread over the entire available part of the coordinate space and show a bizarre nodal pattern (as was anticipated in the Experimental Section). In other words, the fragmentation of NO$_2$ is state-specific but not mode-specific.

We estimate the degree of overlap of the resonances by means of the parameter $\xi = \langle \Gamma \rangle \rho$, with $\langle \Gamma \rangle$ being the "local" average width in a narrow energy interval. If $\xi \ll 1$ the resonances are isolated and nonoverlapping. If $\xi \gg 1$, the resonances strongly overlap. Without showing the result of this assessment, we mention that for the first, better converged set of resonances ξ is about unity just at threshold and then gradually increases to $\xi \approx 3$ at 1000 cm^{-1}. Note, however, that a more natural characteristic of interaction between two resonance states is the overlap integral between their wave functions, which is zero if resonances are completely independent and isolated. This aspect is discussed in the next subsection and in paper II.

Also shown in Figure 1 is the SACM rate calculated as described in section III. It rises steeply in the vicinity of the threshold energy and after about 200 cm^{-1} increases more gradually with energy. The average rate, $\langle k_{\text{qm}} \rangle$, computed with the better converged resonances is noticeably smaller than k_{SACM}. Of course, by gradually including broader resonances, one can always find a set of resonances, for which the average is close to k_{SACM}. In particular, averaging over all resonances with $\Gamma \leq \Gamma_{\text{max}}$ gives an average rate, which is in very good agreement with the SACM prediction.

The relationship between the average quantum rate $\langle k_{\text{qm}} \rangle$ and the statistical rate k_{TST} was discussed by Peskin et al. in ref 57. Within the framework of a random matrix model, the statistical rate was shown to be always smaller than $\langle k_{\text{qm}} \rangle$ if the resonances strongly overlap. Figure 1 demonstrates that such "saturation" of the decay rate is not observed in our calculations; instead, $k_{\text{TST}} \geq \langle k_{\text{qm}} \rangle$. Conceivably, the reason is that the overlap parameter ξ in NO$_2$ is only moderately large near threshold.

C. Theoretical Decay Curves and Comparison with Experimental Data. Because it is impossible to extract dissociation rates of individual states from the experimental decay

curves, we have to calculate theoretical time-dependent signals and compare them with the experimental counterparts. The most direct strategy would be (1) to prepare the molecule in the initial vibrational state in the electronic ground state, (2) to excite the molecule from the X̃ to the Ã state (see Chapter 16 in ref 7) by employing a laser pulse, which has the same carrier frequency and length as in the experiment, and (3) to calculate the norm of the wave packet as a function of time. Such a scheme requires knowledge of the transition dipole moment function, the upper-state PES, and the nonadiabatic coupling from the Ã state to the ground state X̃. Since this information is not available to us at the present time,[58] we have to model the dissociation process in an approximate way—by means of the resonance widths Γ_n. We exploit the fact that the amplitudes of the experimental signals (Figure 3) at time Δt are proportional to the population of molecules, whose internal energy is larger than the dissociation energy, but which are not yet dissociated.

According to the basic assumptions described in section III, we suppose that the excitation with the pump pulse and the subsequent nonadiabatic transition from the excited to the ground electronic state prepares a superposition of metastable vibrational states $|\psi_n\rangle$ on the ground-state PES,

$$|\Phi(0)\rangle = \sum_n A_n |\psi_n\rangle \qquad (5)$$

where the energy dependence of the coefficients A_n resemble the spectral shape of the laser pulse (see below). The fraction of NO_2 molecules, which by the time t are still intact, is given by the integral of the square of $\Phi(t)$ over the inner part of the potential. It is this time-dependent quantity that we want to compare with the experimental decay curves. The $|\psi_n\rangle$'s are the resonance states of the Hamiltonian $\hat{H}_{opt}(E)$ in eq 3. Their time dependence is given by the usual factor $\exp(-iE_n t/\hbar)$ − with E_n being complex for the resonance states. The Hamiltonian $\hat{H}_{opt}(E)$ is not Hermitian, and through the optical potential, it is energy dependent. Consequently, the resonance wave functions for two different energies are, in general, *nonorthogonal*, and therefore one has to know the overlap integrals between all resonance states included in the wave packet, when the decay curves are to be calculated. This enormously complicates the calculation and requires information we do not possess. However, under certain conditions, which, as we believe, are met for NO_2 and which are discussed in paper II, the states can be considered to be *approximately (bi)orthogonal*. The main argument is that all resonance poles lie close to the real energy axis, irrespective of the large fluctuations. Thus, the resonances are nearly independent of each other, although the overlap parameter ξ is larger than 1.

Assuming bi-orthogonality the probability amplitude for finding the molecule in the nth state is given by

$$p_n = \langle\tilde{\psi}_n|\Phi(t)\rangle = A_n e^{-iE_n t/\hbar} \qquad (6)$$

where $\langle\tilde{\psi}_n|$ is the dual state to $|\psi_n\rangle$ (see paper II). The survival probability, i.e., the probability of finding the molecule in any state in the interaction region is determined by

$$P(t) = \sum_n |p_n|^2 = \sum_n |A_n|^2 e^{-\Gamma_n t/\hbar} \qquad (7)$$

This equation allows us to approximately calculate the decay of the population of bound NO_2 molecules using information only about dissociation rates, without explicit calculation of the resonance wave functions.

In ref 4 (Figure 16) we compared, for the dissociation of HNO, the time dependence of the norm of an actually propagated wave packet with $P(t)$ from eq 7 and perfect agreement was obtained. However, the comparison between HNO and NO_2 as far as the applicability of eq 7 is concerned must be considered with some caution, because the overlap parameter ξ is larger in the case of NO_2.

With eq 7, we model not only quantum time-dependent decay curves but also SACM ones. In the case of the statistical theory, eq 7 is an ad hoc assumption that enables one to incorporate the variation of $k_{SACM}(E)$ in the energy windows spanned by the laser pulses. The sum in eq 7 then effectively runs over SACM open channels with energies falling inside the laser bandwidth.

The coefficients $|A_n|^2$ are defined by

$$|A_n|^2 = |a_n|^2 e^{-\alpha(\bar{E} - E_n^0)^2} \qquad (8)$$

The $|a_n|^2$ are vibrational Franck−Condon factors, assumed to be the same for all states; a random distribution does not noticeably change the results. The Gaussian factor describes the spectral profile of the pump laser pulse, with $\bar{E}$ denoting the mean excess energy. The exponent α is set to 6.9×10^{-5} cm^2 corresponding to a full width at half-maximum (fwhm) of 200 cm^{-1}. Three of the four energy ranges, in which resonance states are excited by the different pump pulses, are indicated in Figure 1 ($\bar{E}$ = 124, 712, and 982 cm^{-1}). It is evident that in the experiment many resonances are coherently excited; i.e., many exponential factors contribute to the decay curves. Finally, the theoretical survival probabilities $P(t)$ from eq 7 are convoluted with the experimental time resolution,

$$\tilde{P}(t) = \int_0^\infty P(\tau)\, e^{-\beta(t-\tau)^2}\, d\tau \qquad (9)$$

The Gaussian in eq 9 ($\beta = 6.6 \times 10^{-6}$ fs^{-2}) has a fwhm of 650 fs. The convoluted decay curves are normalized to their maximum values and slightly shifted, so that the maximum is attained at $t = 0$. This shift never exceeds 0.5 ps. All resonances shown in Figure 1 are taken into account, provided $\Gamma \leq \Gamma_{max}$ of eq 4. Excluding the less well converged resonances only slightly affects the decay curves at short times; i.e., the initial decay becomes a bit slower.

The theoretical decay curves are compared with the experimental ones in Figure 3. For the linear representation the experimental long-time asymptote is added to the theoretical curves. On the linear scale, both theoretical predictions, $\tilde{P}_{qm}(t)$ and $\tilde{P}_{SACM}(t)$, agree satisfactorily with the experimental results. The logarithmic representation, however, reveals noticeable differences between the two theories. For the short-time branches for $\bar{E} = 0$ and 124 cm^{-1} ($t \leq 2$−4 ps) SACM provides a better fit to experimental data points. The quantum mechanical calculations underestimate the decay rate—the density of calculated broad resonances is, obviously, too low. Furthermore, the convolution in eq 9 tends to suppress the contributions of states with large k_n. Note that in the initial stage the decay can be fairly well approximated by a single exponent. The slight curvature of the SACM curve in the logarithmic representation stems for the energy dependence of $k_{SACM}(E)$, which is particularly strong close to threshold.

The nonexponentiality of the decay becomes pronounced at longer times, after 60%−90% of the molecules excited above D_0 have dissociated. The SACM curves fall off too rapidly in this region and the energy dependence of $k_{SACM}(E)$ is unable to explain the nonexponential decay. Because of the many rates

that are drastically smaller than the statistical rate, the quantum mechanical curves necessarily decay more slowly than the statistical ones. It is in this time regime that the slopes of the quantum and the experimental signals agree best. This observation confirms, beyond any doubt, that the wave packet prepared by the pump laser pulse contains states with rates considerably smaller than the SACM rate. On the other hand, quantum mechanical rates, which are significantly larger than k_{SACM}, affect the decay curves only at very small times, where due to the convolution and the assumptions concerning the preparation of the wave packet the comparison with experiment is questionable anyhow. The more rapid decay at higher excess energy indicates that the number of extremely narrow resonances, with $k_{qm} \ll k_{SACM}$, decreases with energy. A molecule with much less chaotic character (i.e., more pronounced *mode specificity*), like HOCl, for example,[12] would have very narrow resonances even high above threshold.

The theoretical decay curves remain nonexponential even if the size of the energy window, in which resonances are excited, is significantly reduced. We recalculated $P(t)$ with the exponent α in eq 8 corresponding to a fwhm of 30 cm^{-1} and again found nonexponential decay. The same will be, of course, true of any other energy window much wider than the average spacing between adjacent resonance states (which is about 1 cm^{-1} in our calculations).

D. Distribution of Resonance Widths. The intramolecular dynamics of NO$_2$ is irregular and therefore it appears reasonable to compare the distribution of dissociation rates with the predictions of statistical theories. Random matrix theory (RMT), developed in the context of nuclear reactions,[59] predicts that the widths of isolated resonance states in a small energy window follow a χ^2 distribution, i.e.,

$$Q(k) = \frac{N}{2\langle k \rangle}\left(\frac{Nk}{2\langle k \rangle}\right)^{(N-2)/2}\frac{e^{-Nk/2\langle k \rangle}}{\Gamma\left(\frac{N}{2}\right)} \qquad (10)$$

where $\langle k \rangle$ is the average rate in the particular energy range and $\Gamma(x)$ is the Gamma function. N is the number of open quantum channels; the number of channels used in the SACM approach, $W(E)$ in eq 1, seems to be a sound choice. The larger N, the narrower is the distribution and the smaller is the asymmetry with respect to $\langle k \rangle$. The relation between the statistical prediction, on one hand, and the experimental or the quantum mechanical results, on the other, can be investigated in two ways, which we discuss separately.

The time-resolved decay curves do not yield direct information about the distributions of rates. However, following Miller[60] and Lu and Hase[61] the χ^2 distribution can be transformed into a decay curve according to

$$P(t) = \int e^{-kt} Q(k)\, dk = \left(1 + \frac{2}{N}\langle k \rangle t\right)^{-N/2} \qquad (11)$$

$P(t)$ approaches an exponential in the limit $N \rightarrow \infty$. To compare with the experimental decay curves for a particular excitation energy, we determine an average experimental rate $\langle k \rangle$ and evaluate eq 11 for various values of N. The average experimental rate for each excess energy is determined by fitting the experimental decay curve to a sum of three exponential functions and taking the weighted average of the three resulting rate constants. The results of this comparison for the two lowest excess energies are shown in Figure 4. It is evident that $N = 2$ reproduces in both cases the experimental data very well. Larger values of open channels suppress the smaller rates and therefore
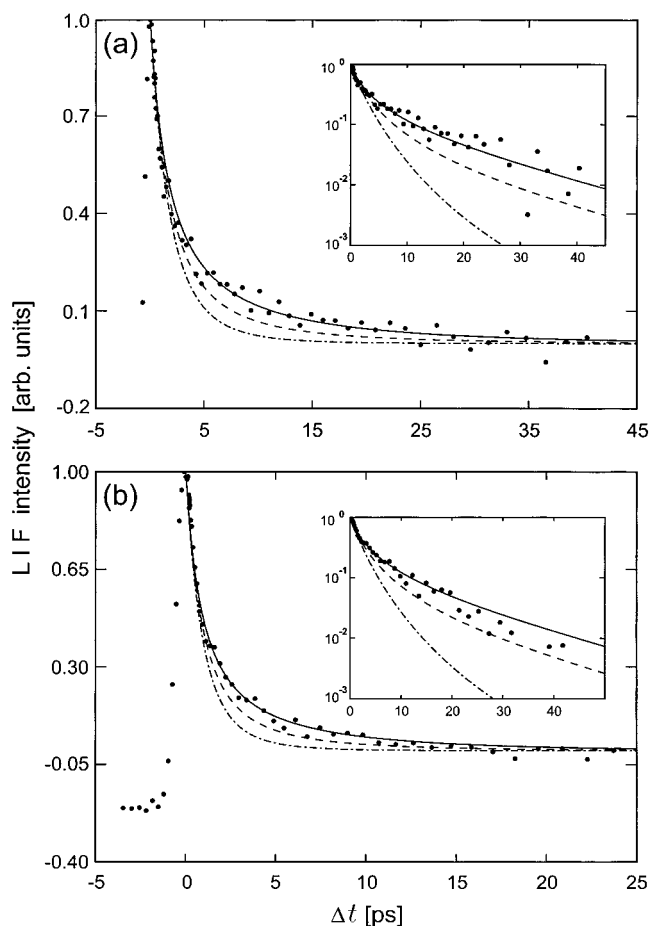

Figure 4. Test of the random matrix theory distribution of rates by comparison with experimental decay curves for $\lambda_{pu} = 398$ nm (a) and 396 nm (b). The number of open channels are $N = 2$ (solid lines), $N = 4$ (dashed lines), and $N = 10$ (dashed−dotted lines). The insets show the same results on a logarithmic scale.

lead to curves, which fall off too quickly. $N = 2$ is significantly smaller than the predicted number of open adiabatic channels, which, for our PES, is about 8 for the average excess energy of 124 cm^{-1}.

For the quantum mechanical calculations we can directly compare the distributions of the calculated rates with the RMT prediction. This is done in Figure 5 for two energy windows. The average excess energies roughly correspond to the experiments with 396 and 383 nm laser light. Only the better converged resonances are taken into account. The distribution for the lower energy window is relatively broad with the majority of rates clearly being smaller than $\langle k \rangle$. It is this large number of extraordinarily small rates that lead to the pronounced multiexponential decay for low excess energies. The distribution for the higher energy window peaks closer to $\langle k \rangle$ and is noticeably narrower than the low-energy distribution. Consequently, the corresponding decay curve can be better represented by a single exponential. In both cases the distributions can be reasonably well fit to a χ^2 form. However, the effective number of open channels obtained from such fits is again significantly smaller than the number of open channels predicted by SACM theory; the best-fit parameter is $N = 4$ for the first energy window and 12 for the second one, while the SACM predictions are 11 and 20, respectively.

In conclusion, the experimental decay curves as well as the calculated dissociation rates are compatible with χ^2 distributions. However, the effective number of open channels must be considered as a fitting parameter, which is, at least for NO$_2$,
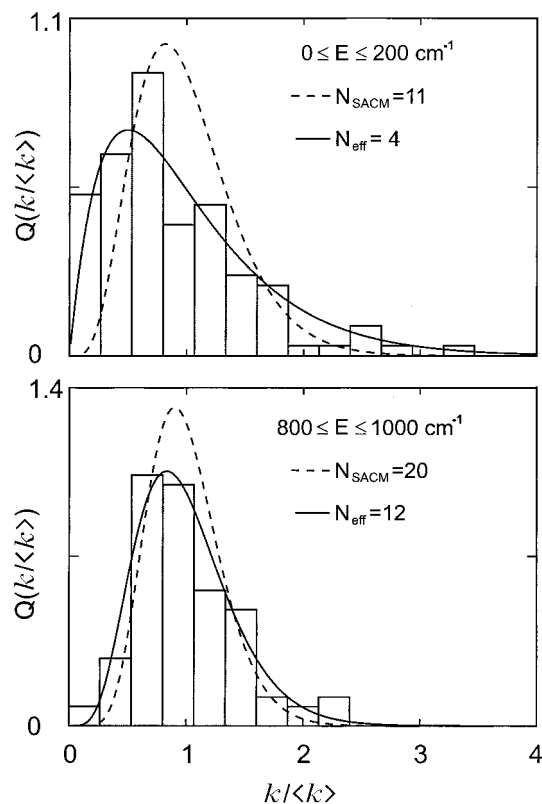
Figure 5. Distributions of theoretical rates, $Q(k/\langle k \rangle)$, in two energy windows as indicated. The solid and broken lines represent χ^2 distributions with different numbers of open channels. N_{SACM} is the number of open channels predicted by SACM theory and N_{eff} is obtained by fitting the calculated distributions.

significantly smaller than the number of open channels derived from the PES according to the SACM approach. A similar observation was previously made by Mandelshtam and Taylor in the dissociation of the H_3^+ molecular ion.[49] A nonstatistical distribution of the transmission coefficients of the open channels may account for this discrepancy. It is concievable that the transmission coefficients ($T_a = 1 - |S_{aa}|^2$, where S_{aa} is the diagonal matrix element of the **S** matrix for a channel a), assumed to be one in SACM, are smaller than one and for some channels even close to zero. We also note that a detailed analysis of the statistical properties of the quantum mechanical resonances for NO_2 would require comparison with a distribution function, which is generalized to the case of overlapping resonances, for example, the distribution recently derived by Fyodorov and Sommers.[62]

E. Comparison with Other Experiments. The range of rates extracted from our previously published frequency-resolved spectrum[20] are indicated by the vertical bar in Figure 1. Because of the strong overlap, line widths could be determined only in a tiny energy window of about 10 cm^{-1} above threshold. The smallest rates measured agree well, within a factor of 2 or so, with the smallest rates calculated. Rates above 1×10^{11} s^{-1}, which correspond to widths larger than 1 cm^{-1}, could not be resolved because of the considerable overlap. The estimated average rate of 2×10^{10} s^{-1} corresponds to a lifetime of about 50 ps and that is roughly the time scale of the decay curves in the 398 nm experiment (see Figure 3).

The fragmentation of NO_2 has been previously investigated by means of time-resolved experiments by Ionov et al.[23] While in the present experiment the decay of the excited-state population of the parent molecule is measured, they detected the appearance of NO fragments in particular quantum states.

Both measurements should give the same dissociation rates and indeed, the *average* rates obtained in our experiment agree, within the experimental error, with the data of Ionov et al.[23] (Figure 1). The result of Ionov et al. near 1000 cm^{-1} seems to indicate a rapid increase of the rate at higher excess energies. However, our experiment at 310 nm ($E \approx 7100$ cm^{-1}, fwhm $\approx$ 180 fs) yields a value of only 3×10^{12} s^{-1}. This suggests that the rate constant gradually approaches a "saturation limit" as E increases beyond 1000 cm^{-1}.

In contrast to our work, Ionov et al.[23] did not observe multiexponential decays; all their appearance curves have been fitted with a single-exponential ansatz. The explanation of this qualitative discrepancy is not completely clear; it could be the different laser bandwidths (or, equivalently, the different time resolutions) used in the two experiments or the better signal-to-noise ratio in our case. In their most recent investigation Bezel et al.[56] tried to estimate how pronounced the nonexponential behavior must be in order to be discernible in their experiment. They added two exponentials with rates differing by a factor of 3 and concluded that the resulting "traces are barely distinguishable." However, this is not a realistic assessment for NO_2: According to our calculations, the rates at threshold vary by about 2 orders of magnitude rather than merely a factor of 3. Adding exponentials according to eq 7 with the calculated quantum mechanical rates gives, beyond any doubt, nonexponential decay curves.

In a most recent set of experiments Bezel et al.[63] excited NO_2 just at threshold with laser pulses having widths of the order of 30 ps, which corresponds to a (Fourier-limited) spectral width of ca. 1 cm^{-1}. What they found are large, order of magnitude variations in the dissociation rate under tiny changes of the excess energy ($\approx$18 cm^{-1}). This observation is in full agreement with our quantum mechanical calculations. Just at threshold, the spacing between neighboring resonances is of the order of 1–2 cm^{-1}. Thus, the laser pulses coherently excite superpositions of only a few resonance states. When the wavelength is varied, the composition of the "wave packet" changes strongly and so does the average rate. The smallest rate in our calculations around the threshold region is 0.015 ps^{-1} and the largest one is 0.25 ps^{-1}. This is exactly the range measured by Bezel et al.[63] Of course, this astonishing agreement must be considered as a mere coincidence. However, the qualitative effect, namely a large variation in a tiny energy range, seems to be nicely confirmed by our calculations.

The threshold rate is often used to estimate the density of states at threshold through $k_{st} = 1/(h\rho)$.[64,65] In view of the large fluctuations at threshold, this can only be considered as a rough, order of magnitude assessment. The lowest (converged) rate near threshold is 0.015 ps^{-1}, which is significantly smaller than the 0.095 ps^{-1} calculated for the SACM rate just above threshold. Averaging over all (converged) resonances in the interval up to the second vibrational state at the transition state ($W = 2$) yields a rate of 0.035 ps^{-1}, which is still about a factor of 3 smaller than the SACM rate. When making these comparisons, one must keep in mind that for numerical reasons resonances right at the opening of the first channel are extremely difficult to converge and therefore not included in these considerations.

Ionov et al.[23] discussed in length the possibility of steps in the variation of $k(E)$ with energy, as predicted by eq 1. The steps would be induced by the opening of the second, the third, etc. bending vibrational state at the transition state, provided the statistical model were correct. Ionov et al.[23] claimed to have observed steps at 100 and 200 cm^{-1}. However, in view of the

large fluctuations of the quantum mechanical rates we find a steplike behavior of an average rate difficult to believe. At the first step the average rate would increase by a factor of 2. On the other hand, the quantum mechanical rates fluctuate by at least a factor of 10 in the low-energy regime. Moreover, the energy increment from one step to the next one is of the order of 10 cm^{-1} at low energies, which is much smaller than the 100 cm^{-1} reported by Ionov et al.[23] We believe that it is unlikely that the angular dependence at intermediate and large O$-$NO distances, which is responsible for the buildup of barriers in the adiabatic potential curves, is so incorrectly reproduced by our PES that the bending frequency at the transition state is underestimated by 1 order of magnitude.

V. Summary

(1) The unimolecular dissociation of NO$_2$ molecules excited above the first threshold, have been studied by means of a time-resolved pump$-$probe experiment. The dissociative decay is nonexponential with the deviations from single-exponential behavior being most pronounced between 1 and 10 ps, depending on the energy, after excitation with the pump pulse.

(2) Quantum mechanical state-specific dissociation rates, calculated on an ab initio adiabatic potential energy surface, fluctuate over more than 2 orders of magnitude around the average value. The width of the distribution of dissociation rates is largest at the threshold and slowly decreases with increasing excess energy.

(3) The observed nonexponential decay is due to the simultaneous excitation of many resonance states by the pump pulse, which subsequently decay with individual rate coefficients. The multiexponential decay curves calculated by using the quantum mechanical rates are in good agreement with the experimental curves, especially at longer times. The statistical adiabatic channel model, employing the same ab initio potential energy surface, adequately describes the initial short-time decay, which can be well described by a single exponential. However, it fails to predict the slow long-time dissociation, which is due to the narrow resonances.

(4) The distribution of resonance widths is close to a χ^2 distribution. However, the effective number of open channels is found to be significantly smaller than the number of open channels predicted by the statistical adiabatic channel model.

(5) The quantum mechanical calculations provide a realistic overall picture of the dissociation dynamics of NO$_2$. They adequately reproduce all experimental results concerning the dissociation rate: the range of the lowest rates near the threshold extracted from the energy-resolved spectroscopic experiments, the average widths up to 1000 cm^{-1} above threshold obtained in the previous and the present time-resolved measurements, the nonexponential decay observed in the present experiments, and the large changes over a very small energy interval near threshold.

Supporting Information Available: All quantum mechanical dissociation rates and the SACM results discussed in section IVB are available free of charge via the Internet at http://pubs.acs.org.

References and Notes

(1) Laidler, K. J. *Theories of Chemical Reaction Rates*; McGraw-Hill: New York, 1969.

(2) Baer, T.; Hase, W. L. *Unimolecular Reaction Dynamics*; Oxford University Press: Oxford, U.K., 1996.

(3) Hase., W. L. In *Modern Theoretical Chemistry, Dynamics of Molecular Collisions*; Miller, W. H., Ed.; Plenum: New York, 1976; Part B.

(4) Schinke, R.; Beck, C.; Grebenshchikov, S.; Keller, H.-M. *Ber. Bunsen-Ges. Phys. Chem.* **1998**, *102*, 593.

(5) Bowman, J. M. *J. Phys. Chem. A* **1998**, *102*, 3006.

(6) Landau, L. D.; Lifshitz, E. M. *Quantum Mechanics. Nonrelativistic Theory*; Pergamon: New York, 1976.

(7) Schinke, R. *Photodissociation Dynamics*; Cambridge University Press: Cambridge, U.K., 1993.

(8) Miller, W. H. *Chem. Rev.* **1987** *87*, 19.

(9) Tobiason, J. D.; Dunlop, J. R.; Rohlfing, E. A. *J. Chem. Phys.* **1995**, *103*, 1448.

(10) Keller, H.-M.; Flöthmann, H.; Dobbyn, A. J.; Schinke, R.; Werner, H.-J.; Bauer, C.; Rosmus, P. *J. Chem. Phys.* **1996**, *105*, 4983.

(11) Skokov, S.; Bowman, J. M.; Mandelstam, V. A. *Phys. Chem. Chem. Phys.* **1999**, *1*, 1279.

(12) Hauschildt, J.; Weiss, J.; Beck, C.; Grebenshchikov, S. Yu.; Düren, R.; Schinke, R.; Koput, J. *Chem. Phys. Lett.* **1999**, *300*, 569.

(13) Green, W. H., Jr.; Moore, C. B.; Polik, W. F. *Annu. Rev. Phys. Chem.* **1992**, *43*, 591.

(14) Stöck, C.; Li, X.; Keller, H.-M.; Schinke, R.; Temps, F. *J. Chem. Phys.* **1997**, *106*, 5333.

(15) Dertinger, S.; Geers, A.; Kappert, J.; Wiebrecht, J.; Temps, F. *Faraday Discuss. Chem. Soc.* **1995**, *102*, 31.

(16) Dutton, G.; Barnes, R. J.; Sinha, A. *J. Chem. Phys.* **1999**, *111*, 4976.

(17) Callegari, A.; Rebstein, J.; Jost, R.; Rizzo, T. R. *J. Chem. Phys.* **1999**, *111*, 7359.

(18) Reiche, F.; Abel, B.; Beck, R. D.; Rizzo, T. R. *J. Chem. Phys.* **2000**, *112*, 8885.

(19) Miyawaki, J.; Yamanouchi, K.; Tsuchiya, S. *J. Chem. Phys.* **1993**, *99*, 254.

(20) Abel, B.; Hamann, H. H.; Lange, V. *Faraday Discuss. Chem. Soc.* **1995**, *102*, 147.

(21) Manz, J.; Wöste, L., Eds.; *Femtosecond Chemistry*; Verlag Chemie: Weinheim, 1995.

(22) Khundkar, L. R.; Zewail, A. H. *Annu. Rev. Phys. Chem.* **1990**, *41*, 15. Zewail, A. H. *Faraday Discuss. Chem. Soc.* **1991**, *91*, 207.

(23) Ionov, S. I.; Bruckner, G. A.; Jaques, C.; Chen, Y.; Wittig, C. *J. Chem. Phys.* **1993**, *99*, 3420.

(24) Grebenshchikov, S. Yu.; Beck, C.; Flöthmann, H.; Schinke, R.; Kato, S. *J. Chem. Phys.* **1999**, *111*, 619.

(25) Reid, S. A.; Reisler, H. *Annu. Rev. Phys. Chem.* **1996**, *47*, 495.

(26) Smalley, R. E.; Wharton, L.; Levy, D. H. *J. Chem. Phys.* **1975**, *63*, 4977.

(27) Busch, G. E.; Wilson, K. R. *J. Chem. Phys.* **1972**, *56*, 3626; *Ibid.* **1972**, *56*, 3638.

(28) Robra, U.; Zacharias, H.; Welge, K. *Z. Phys. D* **1990**, *16*, 175.

(29) Reid, A. A.; Reisler, H. *J. Chem. Phys.* **1994**, *101*, 5683; *J. Phys. Chem.* **1996**, *100*, 474.

(30) Harrison, J. A.; Yang, X.; Rösslein, M.; Felder, P.; Huber, J. R. *J. Phys. Chem.* **1994**, *98*, 12260.

(31) Mueller, J. A.; Rogers, S. A.; Houston, P. L. *J. Phys. Chem.* **1998**, *102*, 9666.

(32) Gaedtke, H.; Hippler, H.; Troe, J. *Chem. Phys. Lett.* **1972**, *16*, 177.

(33) Mons, M.; Dimicoli, I. *Chem. Phys.* **1989**, *130*, 307.

(34) Monti, O. L. A.; Dickinson, H.; Mackenzie, S. R.; Softley, T. P. *J. Chem. Phys.* **2000**, *112*, 3699.

(35) Hirsch, G.; Buenker, R. J.; Petrongolo, C. *Mol. Phys.* **1991**, *73*, 1085.

(36) Leonardi, E.; Petrongolo, C.; Keshari, V.; Hirsch, G.; Buenker, R. J. *Mol. Phys.* **1994**, *82*, 553.

(37) Leonardi, E.; Petrongolo, C.; Hirsch, G.; Buenker, R. J. *J. Chem. Phys.* **1996**, *105*, 20.

(38) Salzgeber, R. F.; Mandelshtam, V. A.; Schlier, Ch.; Taylor, H. S. *J. Chem. Phys.* **1998**, *109*, 937.

(39) Salzgeber, R. F.; Mandelshtam, V. A.; Schlier, Ch.; Taylor, H. S. *J. Chem. Phys.* **1999**, *110*, 3756.

(40) Santoro, F.; Petrongolo, C. *J. Chem. Phys.* **1999**, *110*, 4419.

(41) Klippenstein, S. J.; Radivoyevitch, T. *J. Chem. Phys.* **1993**, *99*, 3644.

(42) Harding, L. B.; Stark, H.; Troe, J.; Ushakov, V. G. *Phys. Chem. Chem. Phys.* **1999**, *1*, 63.

10408 *J. Phys. Chem. A, Vol. 104, No. 45, 2000*

Kirmse et al.

(43) Grebenshchikov, S. Yu. *J. Phys. Chem.* **2000**, *104*, 10409, following paper.

(44) Bigio, L.; Grant, E. R. *J. Chem. Phys.* **1985**, *83*, 5361; *Ibid*. **1987**, *87*, 360.

(45) Lehmann, K. K.; Coy, S. L.; *J. Chem. Phys.* **1985**, *83*, 3290; Coy, S. L.; Lehmann, K. K.; DeLucia, F. C. *J. Chem. Phys.* **1986**, *85*, 4297.

(46) Haller, E.; Köppel, H.; Cederbaum, L. S. *J. Mol. Spectrosc.* **1985**, *111*, 377.

(47) Mandelshtam, V. A.; Taylor, H. S. *J. Chem. Phys.* **1995**, *103*, 2903.

(48) Kroes, G.-J.; Wall, M. R.; Pang, J. W.; Neuhauser, D. *J. Chem. Phys.* **1997**, *106*, 1800.

(49) Mandelshtam, V. A.; Taylor, H. S. *J. Chem. Soc., Faraday Trans.* **1997**, *93*, 847.

(50) Light, J. C. In *Time-Dependent Quantum Molecular Dynamics*; Broeckhove, J.; Lathouwers, L., Eds.; Plenum Press: New York, 1992.

(51) Harris, D. O.; Engerholm, G. G.; Gwinn, W. D. *J. Chem. Phys.* **1965**, *43*, 1515.

(52) Grebenshchikov, S. Yu.; Schinke, R.; Mandelshtam, V. A. Manuscript in preparation.

(53) Quack, M.; Troe, J. *Ber. Bunsen-Ges. Phys. Chem.* **1974**, *78*, 240.

(54) In contrast to what is stated below eq 6 in ref 24 the energy is given in eV rather than cm^{-1}. In addition, E in eq 6 is measured with respect to the classical threshold O + NO(r_e), whereas $E^\dagger$ in Figure 3 of ref 24 is measured with respect to the quantum mechanical threshold O + NO($n = 0$).

(55) In ref 56 it is argued that the nonexponential behavior of our decay curves is "due in large part to the fact that a significant fraction of the molecules were excited to energies below D_0." This is not true. Naturally, in the logarithmic representations the asymptotic values of the decay curves, which are due to the bound molecules, are subtracted.

(56) Bezel, I.; Ionov, P.; Wittig, C. *J. Chem. Phys.* **1999**, *111*, 9267.

(57) Peskin, U.; Reisler, H.; Miller, W. H. *J. Chem. Phys.* **1994**, *101*, 9672.

(58) Calculations of global potential energy surfaces for the two lowest states, the transition dipole moment function, and the coupling elements are presently underway. Once these quantities are available the excitation and dissociation of NO$_2$ can be treated in full rigor.

(59) Brody, T. A.; Flores, J.; French, J. B.; Mello, P. A.; Pandey, A.; Wong, S. S. M. *Rev. Mod. Phys.* **1981**, *53*, 385.

(60) Miller, W. H. *J. Chem. Phys.* **1988**, *92*, 4261.

(61) Lu, D.-h.; Hase, W. L. *J. Chem. Phys.* **1989**, *90*, 1557.

(62) Fyodorov, Y. V.; Sommers, H.-J. *J. Math. Phys.* **1997**, *38*, 1918.

(63) Bezel, I.; Stolyarov, D.; Wittig, C. *J. Phys. Chem. A* **1999**, *103*, 10268.

(64) Wittig, C.; Ionov, S. I. *J. Chem. Phys.* **1994**, *100*, 4714.

(65) Miyawaki, J.; Yamanouchi, K.; Tsuchiya, S. *J. Chem. Phys.* **1994**, *100*, 4716.